

**Two-electron photoemission spectroscopy in topological superconductors**Ka Ho Wong <sup>1</sup>, Ameya Patwardhan,<sup>2,3</sup> Peter Abbamonte,<sup>2,3</sup> Fahad Mahmood,<sup>2,3</sup> and Dirk K. Morr <sup>1</sup><sup>1</sup>*Department of Physics, University of Illinois at Chicago, Chicago, Illinois 60607, USA*<sup>2</sup>*Department of Physics, University of Illinois at Urbana-Champaign, Urbana, Illinois 61801, USA*<sup>3</sup>*Materials Research Laboratory, University of Illinois at Urbana-Champaign, Urbana, Illinois 61801, USA* (Received 21 October 2022; revised 22 January 2024; accepted 23 January 2024; published 4 March 2024)

We demonstrate that the photoelectron counting rate,  $P^{(2)}$ , measured in two-electron coincidence spectroscopy experiments, provides insight into the nature of topological superconductivity. In particular, we show that the spin dependence of  $P^{(2)}$  allows one to detect superconducting spin-triplet correlations that are induced in a topological superconductor even in the absence of an associated triplet superconducting order parameter. This ability to detect spin-triplet correlations allows one to distinguish between two recently proposed scenarios for the microscopic origin of topological superconductivity in  $\text{FeSe}_{0.45}\text{Te}_{0.55}$ . Finally, we show that  $P^{(2)}$  exhibits a characteristic intensity maximum that can be employed to detect topological phase transitions.

DOI: [10.1103/PhysRevB.109.094503](https://doi.org/10.1103/PhysRevB.109.094503)**I. INTRODUCTION**

Topological superconductors harbor Majorana zero modes (MZMs) whose non-Abelian statistics in combination with their topological protection against disorder and decoherence effects provide an exciting platform for the realization of topological quantum computing [1]. However, the experimental observation and identification of MZMs in a variety of superconducting systems [2–11] met significant challenges due to the systems' small superconducting gaps, which are often only of the order of a few hundred  $\mu\text{eV}$ . The recent report of topological superconductivity in the iron-based superconductor  $\text{FeSe}_{0.45}\text{Te}_{0.55}$  [12–21], possessing a significantly larger superconducting gap of a few meV, might therefore provide a more suitable platform for the unambiguous identification of MZMs, and the realization of topology based devices and topological quantum computing.

The origin of topological surface superconductivity in  $\text{FeSe}_{0.45}\text{Te}_{0.55}$  was initially proposed to arise from band inversion [12,22–24]—rendering  $\text{FeSe}_{0.45}\text{Te}_{0.55}$  a three-dimensional topological insulator—and the gapping of the ensuing surface Dirac cone by proximity induced superconductivity. We refer to this as the 3DTI mechanism, giving rise to a Fu-Kane like topological superconductor [25]. However, the recent experimental observation of ferromagnetism on the surface of  $\text{FeSe}_{1-x}\text{Te}_x$  [13–15,26] has shed doubts on this interpretation, as topological superconductivity arising from the 3DTI mechanism, being protected by a time reversal symmetry, is destroyed already for rather weak surface ferromagnetism [27,28]. A competing scenario was therefore proposed [28–30] in which the very ferromagnetism observed experimentally in combination with the two-dimensional nature of superconductivity in  $\text{FeSe}_{0.45}\text{Te}_{0.55}$  and a Rashba spin-orbit interaction on the surface induced by the broken inversion symmetry gives rise to topological surface superconductivity (we refer to this as the 2DTSC mechanism).

Clearly, further experiments are required to distinguish between these two proposed scenarios [28].

In this paper, we demonstrate that the photoelectron counting rate [31],  $P^{(2)}$ , measured in two-electron coincidence spectroscopy ( $2e$ -ARPES) experiments, can provide insight into the nature of topological superconducting phases, and thus identify the microscopic origin of topological superconductivity in  $\text{FeSe}_{0.45}\text{Te}_{0.55}$ . In  $2e$ -ARPES experiments, the absorption of a single photon leads to the emission of two coincident photoelectrons. As previously shown [32], the energy dependence of  $P^{(2)}$  can reveal not only the total center of mass momentum of a Cooper pair, but also its spin state. As a result,  $2e$ -ARPES experiments can identify superconducting spin-triplet correlations which are induced within the 2DTSC mechanism in  $\text{FeSe}_{1-x}\text{Te}_x$ , but are all but absent in the 3DTI mechanism. In addition, we show that  $2e$ -ARPES experiments can identify topological phase transitions which coincide with a maximum in  $P^{(2)}$  for photoelectrons with equal spin. These results open an avenue to distinguish between proposed mechanisms for the emergence of topological superconductivity in  $\text{FeSe}_{1-x}\text{Te}_x$ .

**II. THEORETICAL MODEL**

In the following, we consider the  $2e$ -ARPES photoelectron counting rate for two different types of topological superconductors: (i) a two-dimensional topological superconductor with broken time reversal symmetry, as described by the 2DTSC mechanism, and (ii) a topological superconductor on the surface of a three-dimensional topological insulator, arising from the proximity coupling of its surface Dirac cone to an  $s$ -wave superconductor, as described by the 3DTI mechanism. The former system is described by the

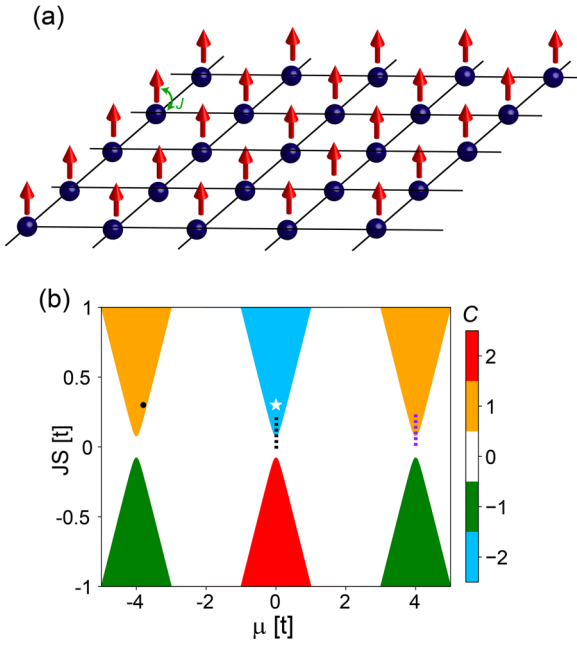


FIG. 1. (a) Schematic representation of the 2DTSC with local magnetic moments interacting with conduction electrons on the surface of an  $s$ -wave superconductor. (b) Topological phase diagram of the 2DTSC in terms of the Chern number  $C$  in the  $(\mu, JS)$  plane for  $(\alpha, \Delta_0) = (0.05, 0.08)t$ .

Hamiltonian [29,33–35]

$$H_{SC} = \sum_{\mathbf{k}} \left[ \xi_{\mathbf{k}} c_{\mathbf{k},\sigma}^\dagger c_{\mathbf{k},\sigma} + \Delta_0 (c_{\mathbf{k},\uparrow}^\dagger c_{-\mathbf{k},\downarrow}^\dagger + c_{-\mathbf{k},\downarrow} c_{\mathbf{k},\uparrow}) + 2\alpha \sum_{\delta,\sigma,\sigma'} \sin(\mathbf{k} \cdot \delta) c_{\mathbf{k},\sigma}^\dagger (\delta \times \sigma)_{\sigma\sigma'}^z c_{\mathbf{k},\sigma'} - JS \sum_{\sigma,\sigma'} c_{\mathbf{k},\sigma}^\dagger \sigma_{\sigma\sigma'}^z c_{\mathbf{k},\sigma'} \right]. \quad (1)$$

Here,  $c_{\mathbf{k},\sigma}^\dagger$  creates an electron with momentum  $\mathbf{k}$  and spin  $\sigma$  and  $\xi_{\mathbf{k}} = -2t(\cos k_x + \cos k_y) - \mu$  is the tight binding dispersion with  $-t$  being the nearest neighbor hopping amplitude, and  $\mu$  being the chemical potential. Moreover,  $\Delta_0$  is the  $s$ -wave superconducting order parameter,  $\alpha$  is the Rashba spin-orbit interaction with  $\delta$  being the unit vector connecting nearest neighbor sites, and  $J$  is the magnetic exchange coupling between the ordered moments of magnitude  $S$  and the conduction electrons. A schematic representation of the 2DTSC is shown in Fig. 1(a). This topological superconductor is in the topological class D, and its topological invariant is the Chern number [35],  $C$ . Below, we consider parameter sets  $(\alpha, \Delta_0, JS)$  that yield a superconducting gap of  $\Delta_{SC} \approx 3.5$  meV, which is similar to that observed in  $\text{FeSe}_{1-x}\text{Te}_x$  [21,36]. The resulting topological phase diagram in terms of  $C$  is shown in Fig. 1(b) in the  $(\mu, JS)$  plane. Note that a similar Hamiltonian has been discussed in the context of cold atom systems [37] and semiconductor heterostructures [38].

The Hamiltonian of the 3DTI system is given by [39]

$$H_{3D} = -t \sum_{\mathbf{r}, j=1,2,3} \left( \Psi_{\mathbf{r}+\hat{e}_j}^\dagger \frac{\Gamma^1 - i\Gamma^{j+1}}{2} \Psi_{\mathbf{r}} + \text{H.c.} \right) + m \sum_{\mathbf{r}} \Psi_{\mathbf{r}}^\dagger \Gamma^1 \Psi_{\mathbf{r}} \quad (2)$$

with spinor

$$\Psi_{\mathbf{r}}^\dagger = (c_{\mathbf{r},1,\uparrow}^\dagger, c_{\mathbf{r},2,\uparrow}^\dagger, c_{\mathbf{r},1,\downarrow}^\dagger, c_{\mathbf{r},2,\downarrow}^\dagger), \quad (3)$$

where  $c_{\mathbf{r},a,\sigma}$  annihilates an electron with spin  $\sigma$  in orbital  $a = 1, 2$  at site  $\mathbf{r}$ , and  $\Gamma^{(0,1,2,3,4)} = (\mathbb{1} \otimes \mathbb{1}, \mathbb{1} \otimes s_z, -\sigma_y \otimes s_x, \sigma_x \otimes s_x, -\mathbb{1} \otimes s_y)$  with  $\sigma_i$  and  $s_i$  ( $i = x, y, z$ ) being Pauli matrices. Within this model, a topological superconducting phase emerges on the surface of the 3DTI due to proximity coupling to a superconductor, and the ensuing opening of a gap in the 3DTI's surface Dirac cone. The proximity induced superconductivity is described by the Hamiltonian

$$H_{\Delta} = \Delta_0 \sum_{\mathbf{r}, a=1,2} c_{\mathbf{r},a,\uparrow}^\dagger c_{\mathbf{r},a,\downarrow}^\dagger + \text{H.c.}, \quad (4)$$

where  $\Delta_0$  is the induced superconducting order parameter with  $s$ -wave symmetry. We note that to demonstrate the qualitative different form of  $P^{(2)}$  in the 2DTSC and 3DTI systems (see below), it is sufficient to consider for simplicity an  $s$ -wave symmetry of the superconducting order parameter, rather than the  $s_{\pm}$ -wave symmetry found in  $\text{FeSe}_{0.45}\text{Te}_{0.55}$ . A more material specific calculation of  $P^{(2)}$  that also takes into account the multiband structure of  $\text{FeSe}_{0.45}\text{Te}_{0.55}$  [29] is reserved for a future study. In  $2e$ -ARPES spectroscopy, there are two distinct processes in which the absorption of a single photon leads to the ejection of a correlated pair of electrons [31,32,40–46], giving rise to the photoelectron counting rate  $P^{(2)}$ . In the first one, the absorption of a photon results in the excitation of a valence band electron into a free photoelectron state, which subsequently ejects a second valence electron via an electron energy-loss-like scattering event, mediated by the Coulomb interaction. In the second process, the photon first excites a photoelectron from a core level (rather than the conduction band). The resulting core hole is then filled by a valence electron, leading to the emission of a second valence electron through an Auger process. As previously shown [32], both processes lead to a very similar energy, momentum, and spin dependence of  $P^{(2)}$ . However, the use of lower photon energy laser based XUV sources will not allow  $2e$ -ARPES experiments to directly probe core states. Below, we will therefore consider  $P^{(2)}$  as arising from the first process only, which is described by the Hamiltonian

$$H_{\text{scat}} = \sum_{\mathbf{k}, \mathbf{q}, \sigma, \nu} \gamma_{\nu}(\mathbf{q}) d_{\mathbf{k}+\mathbf{q},\sigma}^\dagger c_{\mathbf{k},\sigma} (a_{\mathbf{q},\nu} + a_{-\mathbf{q},\nu}^\dagger) + \sum_{\mathbf{k}, \mathbf{p}, \mathbf{q}, \alpha, \beta} V(\mathbf{q}) d_{\mathbf{k}+\mathbf{q},\alpha}^\dagger d_{\mathbf{p}-\mathbf{q},\beta}^\dagger d_{\mathbf{p},\beta} c_{\mathbf{k},\alpha} + \text{H.c.} \quad (5)$$

Here,  $\gamma_{\nu}(\mathbf{q})$  is the effective electron-photon dipole interaction,  $d_{\mathbf{k},\sigma}^\dagger$  ( $c_{\mathbf{k},\sigma}$ ) creates (destroys) a photoelectron (conduction electron) with momentum  $\mathbf{k}$  and spin  $\sigma$ , and  $V(\mathbf{q}) = V_0/(\mathbf{q}^2 + \kappa^2)$  is the Fourier transform of the (screened) Coulomb interaction, with  $\kappa^{-1}$  being the screening length. Moreover,  $a_{\mathbf{q},\nu}$

destroys a photon with momentum  $\mathbf{q}$  and polarization  $\nu$ . We note that in the 3DTI, possessing two orbitals per site, the  $c$ -electron operators in Eq. (5) acquire an orbital index. Since the qualitative nature of  $P^{(2)}$  does not depend on  $\kappa$  [32], we take for concreteness  $\kappa^{-1} = 10a_0$  for the results shown below. Moreover, as the photon momentum is much smaller than typical fermionic momenta, we set it equal to zero, such that  $\gamma_\nu(\mathbf{q}) = \gamma_0$  is simply a momentum-independent constant.

To compute the photoelectron counting rate in  $2e$ -ARPES experiments, which depends on the two photoelectron momenta and spin projections, we use

$$P^{(2)}(\mathbf{k}'_1, \sigma'_1, \mathbf{k}'_2, \sigma'_2) = \frac{1}{Z} \sum_{a,b} \frac{e^{-\beta E_a}}{\Delta t} |\langle \Psi_b | \hat{S}^{(2)}(\infty, -\infty) | \Psi_a \rangle|^2 \quad (6)$$

where  $Z$  is the partition function, and the initial and final states of the entire system before and after the two-step process,  $|\Psi_a\rangle$  and  $|\Psi_b\rangle$ , are represented by the following product states:

$$\begin{aligned} |\Psi_a\rangle &= |\Phi_a\rangle |1_{\mathbf{q},\nu}\rangle_p |0\rangle_{pe}, \\ |\Psi_b\rangle &= |\Phi_b\rangle |0\rangle_p |1_{\mathbf{k}'_1, \sigma'_1} 1_{\mathbf{k}'_2, \sigma'_2}\rangle_{pe} \end{aligned} \quad (7)$$

where  $|1_{\mathbf{q},\nu}\rangle_p$  is the initial state of the photon with wave vector  $\mathbf{q}$  and polarization  $\nu$ , and  $|1_{\mathbf{k}'_1, \sigma'_1} 1_{\mathbf{k}'_2, \sigma'_2}\rangle_{pe}$  is the final photoelectron state with momenta  $\mathbf{k}'_1, \mathbf{k}'_2$  and spins  $\sigma_1, \sigma_2$ . The sum in Eq. (6) runs over all states  $|\Phi_{a,b}\rangle$  of the topological superconductor,  $\Delta t$  is the time over which the photon beam is incident in the superconductor, and  $\hat{S}^{(2)}$  is the second-order contribution to the  $S$  matrix arising from  $H_{\text{scat}}$ . As previously discussed [32], the photoelectron counting rate can then be written as  $P^{(2)} = V^2 P_{\text{SC}}^{(2)} + V P_{\text{2CP}}^{(2)}$ , where  $V$  is the volume of the system. The first term arises from the breaking of a single Cooper pair, and thus directly reflects the strength of the superconducting condensate, while the second term arises from the breaking of two Cooper pairs. Note that the first term scales as  $V^2$ , while the second term scales as  $V$ , as the probability to find a second Cooper pair from which an electron is ejected is given by  $1/V$ . The explicit forms for  $P^{(2)}$  in the 2DTSC and 3DTI systems are given in Appendices A and B, respectively.

### III. RESULTS

#### A. $P^{(2)}$ in a 2DTSC

We begin by considering the photoelectron counting rate in the topological  $C = 1$  phase of the 2DTSC system [at  $\mu = -3.8t$ , see black circle in Fig. 1(b)], whose Fermi surface in the normal state is shown in Fig. 2(a).  $P^{(2)}$  for two photoelectrons with opposite momenta ( $\mathbf{k}'_1 = -\mathbf{k}'_2$ ) located on the Fermi surface [see filled blue circles in Fig. 2(a)], and opposite spins, is shown in Fig. 2(b), both for the normal and superconducting states. In the normal state, the onset of  $P^{(2)}$  occurs when the energy of the photon is sufficiently large to eject two photoelectrons with energy  $\varepsilon_{\mathbf{k}'_1}$  (which also includes the work function). In the superconducting state,  $P^{(2)}$  exhibits two contributions. The first one is a peak at  $\Delta\omega = \omega_{\mathbf{q}} - 2\varepsilon_{\mathbf{k}'_1} = 0$  which arises from  $P_{\text{SC}}^{(2)}$  and reflects the breaking of a single Cooper pair. This peak is present only

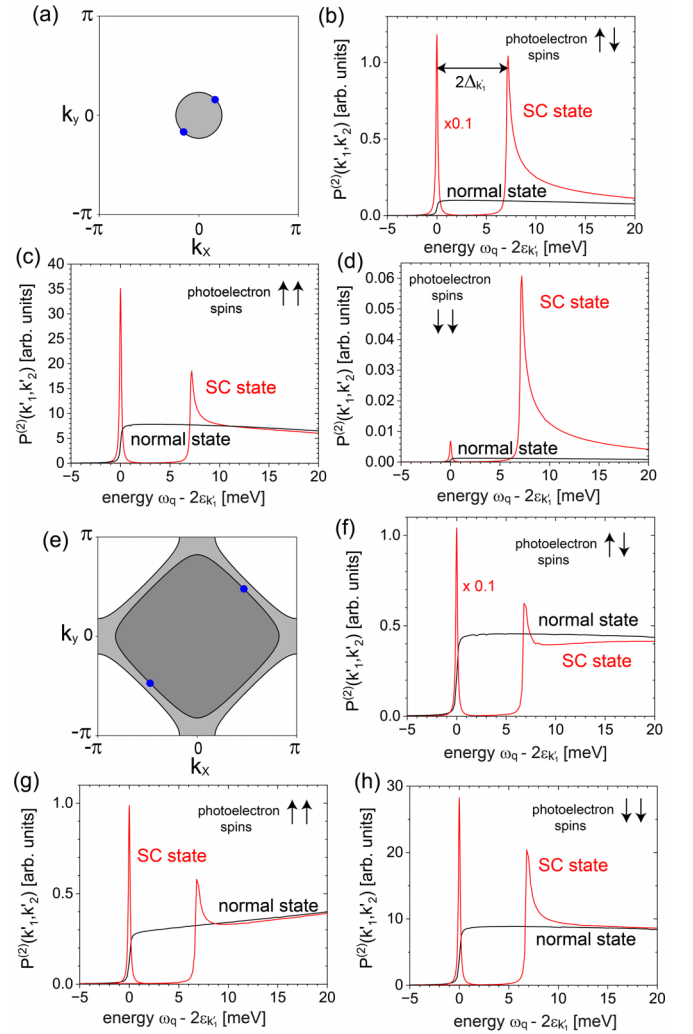


FIG. 2.  $P^{(2)}$  in the topological  $C = 1$  phase at  $\mu = -3.8t$  [black dot in Fig. 1(b)]: (a) Fermi surface in the normal state and (b–d) the corresponding  $P^{(2)}$  for three different spin configurations of the photoelectrons, in the normal (black lines) and superconducting (red lines) states. The photoelectron momenta  $\mathbf{k}'_{1,2}$  are shown as filled blue circles in (a).  $P^{(2)}$  in the topological  $C = -2$  phase at  $\mu = 0$  [white star in Fig. 1(b)]: (e) Fermi surface in the normal state and (f–h) the corresponding  $P^{(2)}$  for three different spin configurations of the photoelectrons, in the normal (black lines) and superconducting (red lines) states. The photoelectron momenta  $\mathbf{k}'_{1,2}$  are shown as filled blue circles in (e). Parameters are  $t = 200$  meV,  $(\alpha, JS) = (0.05, 0.3)t$ , and (b–d)  $\Delta_0 = 0.08t$  and (f–h)  $\Delta_0 = 0.04t$ .

if the two photoelectrons possess the same center of mass momentum and spin state as a Cooper pair [32], as is the case here. The second contribution, arising from  $P_{\text{2CP}}^{(2)}$ , is a continuum with onset energy  $\Delta\omega \approx 2\Delta_{\mathbf{k}'_1}$ , with  $\Delta_{\mathbf{k}'_1}$  being the superconducting gap at  $\mathbf{k}'_1$ , implying that the two measured photoelectrons are ejected from two different Cooper pairs. Moreover, it was previously shown that the emergence of spin-triplet correlations, which are induced by the interplay of ferromagnetism, Rashba spin-orbit interaction, and  $s$ -wave superconductivity, is an essential feature of a 2DTSC [35,47]. To investigate whether these correlations can be probed via  $2e$ -ARPES experiments, we present  $P^{(2)}$

for two photoelectrons possessing equal spins in Figs. 2(c) and 2(d). Interestingly enough, we find that even for this spin configuration, a peak at  $\Delta\omega = 0$  exists. As the starting Hamiltonian, Eq. (5), does not contain a triplet superconducting order parameter, this peak at  $\Delta\omega = 0$  should be attributed to the aforementioned emergence of superconducting spin-triplet correlations.

To gain more insight into the relation between  $P_{SC}^{(2)}$  and the superconducting pairing correlations, we consider the latter in the spin-triplet channel ( $S = 1, S_z = \pm 1$ ), given by  $C_{\mathbf{k},\sigma}^T = \langle c_{\mathbf{k},\sigma}^\dagger c_{-\mathbf{k},\sigma}^\dagger \rangle$  and  $\sigma = \uparrow, \downarrow$ , and the singlet channel ( $S = 0$ ), given by  $C_{\mathbf{k}}^S = \langle c_{\mathbf{k},\uparrow}^\dagger c_{-\mathbf{k},\downarrow}^\dagger - c_{\mathbf{k},\downarrow}^\dagger c_{-\mathbf{k},\uparrow}^\dagger \rangle$ . We note that the superconducting correlations in the spin-triplet channel  $S = 1, S_z = 0$  are identically zero, such that  $P^{(2)}$  for photoelectrons with opposite spins arises solely from the presence of superconducting correlations in the singlet channel. For the same momentum on the Fermi surface [see filled blue circles in Fig. 2(a)] as we considered for the calculation of  $P^{(2)}$  in Figs. 2(b)–2(d), we obtain  $|C_{\mathbf{k},\uparrow}^T| \approx 0.347$ ,  $|C_{\mathbf{k},\downarrow}^T| \approx 0.026$ , and  $C_{\mathbf{k}}^S = 0.252$  (note that  $C_{\mathbf{k},\sigma}^T$  is in general a complex function). Given that  $P_{SC}^{(2)} \sim C^2$  [32], the relative peak intensities in  $P_{SC}^{(2)}$  in the three different channels are in good agreement with the relative strength of the superconducting correlations. This supports our conclusion that  $P_{SC}^{(2)}$  indeed reflects the superconducting correlations in the system. Finally, we note that we obtain qualitatively similar results for  $P^{(2)}$  in the topological  $C = -2$  phase of the 2DTSC [at  $\mu = 0$ , see white star in Fig. 1(b)], whose Fermi surface in the normal state is shown in Fig. 2(e).  $P^{(2)}$  shown in Figs. 2(f)–2(h) exhibits a peak at  $\Delta\omega = 0$  for all three spin configurations, again reflecting the presence of spin-triplet Cooper pairs.

While the presence of spin-triplet correlations is a key feature of a 2DTSC, as shown in Fig. 2, it is not sufficient to uniquely identify a topological phase, as the interplay of ferromagnetism, a Rashba spin-orbit coupling, and an  $s$ -wave superconducting order parameter can also induce spin-triplet correlations in a trivial superconducting phase [35]. The question thus arises whether  $2e$ -ARPES experiments can be employed to distinguish between topological and trivial superconducting phases, or to at least identify topological phase transitions. To answer this question, we consider the topological phase transition between a trivial phase and the topological  $C = -2$  phase, along the black dashed line shown in Fig. 1(b), which is accompanied by the closing of the superconducting gap at the  $X/Y$  points, yielding a gap closing momentum,  $\mathbf{k}_{gc} = (0, \pm\pi), (\pm\pi, 0)$ . We thus consider two photoelectrons with momenta  $\mathbf{k}'_1 = -\mathbf{k}'_2 = \mathbf{k}_{gc}$  and present in Fig. 3(a),  $P_{SC}^{(2)}$  at  $\Delta\omega = 0$  as a function of  $JS$ . As we tune the system through a topological phase transition at  $(JS)_{cr} = \Delta_0$ , we find that while  $P_{SC}^{(2)}$  is nonzero both in the topological and trivial phases, consistent with earlier findings [35], it exhibits a maximum at  $(JS)_{cr}$ . We obtain the same result for the phase transition between a trivial phase and the topological  $C = 1$  phase as shown in Fig. 3(b), along the purple dashed line in Fig. 1(b), where the gap closing occurs at  $\mathbf{k}_{gc} = (\pm\pi, \pm\pi)$ . As before, we find that  $P_{SC}^{(2)}$  reflects the presence of superconducting spin-triplet correlations,  $C_{\mathbf{k},\sigma}^T$ , which also exhibit a peak at the topological phase transition, as shown in Figs. 3(c) and 3(d) for several momenta

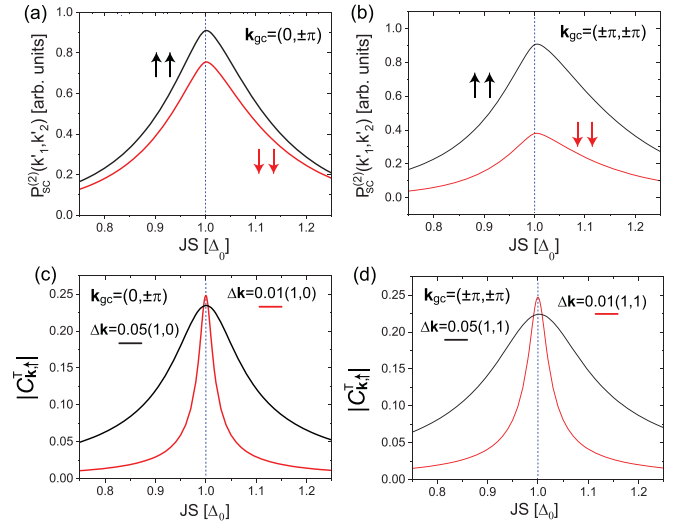


FIG. 3.  $P_{SC}^{(2)}$  at  $\Delta\omega = 0$  for photoelectrons with equal spin projections and momenta  $\mathbf{k}'_1 = -\mathbf{k}'_2 = \mathbf{k}_{gc}$  at the gap closing momentum  $\mathbf{k}_{gc}$ , across a topological phase transition into the (a)  $C = -2$  [ $\mu = 0, \mathbf{k}_{gc} = (0, \pm\pi), (\pm\pi, 0)$ ] and (b)  $C = 1$  [ $\mu = 4t, \mathbf{k}_{gc} = (\pm\pi, \pm\pi)$ ] phases. The vertical dashed blue line indicates the topological phase transition at  $(JS)_{cr} = \Delta_0$ . (c, d)  $|C_{\mathbf{k}}^T|$  for the cases shown in (a) and (b), respectively, for several momenta  $\mathbf{k} = \mathbf{k}_{gc} - \Delta\mathbf{k}$  near  $\mathbf{k}_{gc}$ . Parameters are  $t = 200$  meV and  $(\alpha, \Delta_0) = (0.05, 0.08)t$ .

near  $\mathbf{k}_{gc}$ , corresponding to the cases shown in Figs. 3(a) and 3(b). An analytical expression for the spin-triplet correlations near  $\mathbf{k}_{gc}$  is given in Appendix C, which demonstrates that the increase in  $C_{\mathbf{k},\sigma}^T$  as one approaches the topological phase transition is a direct consequence of the decreasing excitation energy, and hence the gap closing at  $\mathbf{k}_{gc}$ . The fact that  $P_{SC}^{(2)}$  exhibits a maximum at  $(JS)_{cr}$  for both topological phase transitions shown in Figs. 3(a) and 3(b) implies that this maximum is a general signature of topological phase transitions in a 2DTSC, that can be employed to identify them.

### B. $P^{(2)}$ in a 3DTI system

Finally, we consider  $P^{(2)}$  in the topological superconductor arising from the 3DTI mechanism whose surface Dirac cone in the normal state is schematically shown in Fig. 4(a). To this end, we consider a system that is translationally invariant in the  $x$  and  $y$  directions and possesses a finite number of layers  $N_z$  in the  $z$  direction. We assume that photoelectrons are ejected from the surface layer (which contains the Dirac cone) only, as the spectral weight of the Dirac cone on layers below the surface is negligible. Moreover, we assume below that both photoelectrons are of the same orbital character in the 3DTI system (orbital selectivity can in general be achieved by varying the energy or polarization of the incoming photon [48]). However,  $P^{(2)}$  is independent of the orbital from which the photoelectrons are ejected.

In Fig. 4(b), we present  $P^{(2)}$  for photoelectrons ejected from the same orbital with opposite spins and momenta  $\mathbf{k}'_1 = -\mathbf{k}'_2$  on the Fermi surface of the Dirac cone [see filled red cir-

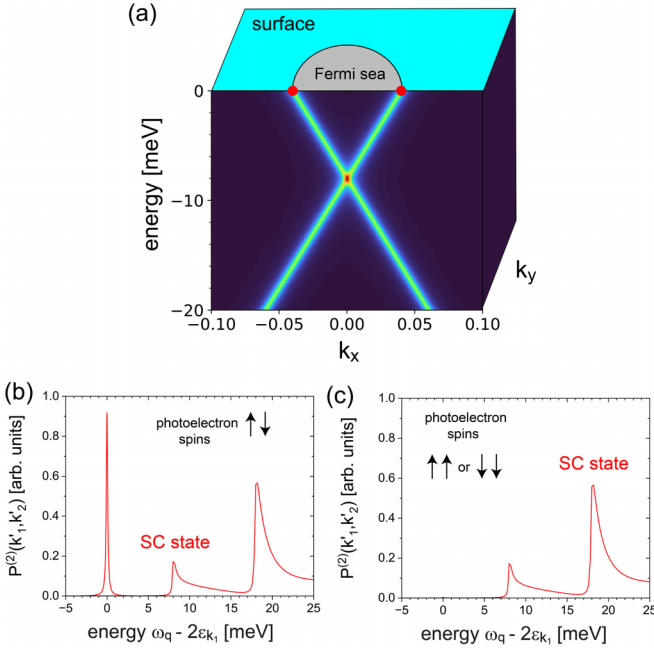


FIG. 4. (a) Schematic representation of a surface Dirac cone in a 3DTI with  $N_z = 5$  layers. (b, c)  $P^{(2)}$  for photoelectrons with momenta indicated by filled red circles in (a) and different spin states. Parameters used here are  $t = 200$  meV and  $(m, \mu, \Delta_0) = (2, 0.04, 0.02)t$ .

cles in Fig. 4(a)]. As expected,  $P^{(2)}$  exhibits a peak at  $\Delta\omega = 0$  arising from the breaking of a single (singlet) Cooper pair, and an onset of a continuum at  $\Delta\omega \approx 2\Delta_{k_i}$  arising from breaking of two Cooper pairs. In contrast, for photoelectrons with the same spin state,  $P^{(2)}$  exhibits a peak at  $\Delta\omega = 0$  whose intensity is more than 500 times smaller [see Fig. 4(c)] than that for the case of opposite photoelectron spins [see Fig. 4(b)]. This is consistent with vanishingly small superconducting correlations  $C_{\mathbf{k},\sigma}^T$  in the triplet  $S = 1, S_z = \pm 1$  channel (as before, the correlations in the  $S = 1, S_z = 0$  channel are identically zero). The reason for the vanishingly small  $C_{\mathbf{k},\sigma}^T$  lies in the helical structure of the surface Dirac cone, reflecting spin momentum locking, which implies that states with opposite momenta  $\mathbf{k}_1 = -\mathbf{k}_2$  possess opposite spin polarizations. As such, these states can only form Cooper pairs in the singlet channel. However, this spin momentum locking, and the associated complete suppression of pairing in the spin-triplet channel, is lifted when the Dirac point is located away from zero energy at nonzero  $E_D$ . Since the degree to which the spin momentum locking is violated scales with  $E_D$ , the spin-triplet correlations and the associated intensities in  $P_{SC}^{(2)}$  remain very small for realistic values of  $E_D$  [12–15], as shown in Fig. 4(c). Thus, in the 3DTI system, the  $\Delta\omega = 0$  peak in  $P_{SC}^{(2)}$  for equal spin configuration is either absent, or at least greatly suppressed in comparison to the peak in  $P_{SC}^{(2)}$  for opposite spin projections, in contrast to the results in the 2DTSC system (see Fig. 2), implying that the presence of ferromagnetism is crucial for the emergence of robust spin-triplet correlations. We thus conclude that the presence or absence of a  $\Delta\omega = 0$  peak in  $P^{(2)}$  for photoelectrons with equal spin states is a characteristic signature of topological superconductivity arising from the 2DTSC and 3DTI mechanisms, respectively, and thus allows us to discriminate between them.

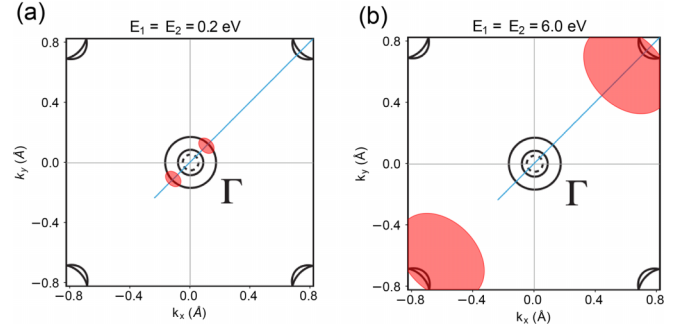


FIG. 5. Schematic form of the Fermi surface of  $\text{FeSe}_{0.5}\text{Te}_{0.5}$  with calculated projections of fields of view (red circles) of two time-of-flight (TOF) analyzers separated by  $90^\circ$ . (a) Calculation done with 0.2-eV kinetic energy of the two electrons (or an incident photon energy of  $h\nu \approx 9$  eV), corresponding to electrons from the holelike Fermi surface. (b) Calculation done with 6.0-eV kinetic energy of the two electrons (or an incident photon energy of  $h\nu \approx 21$  eV), corresponding to electrons from the electronlike Fermi surface. (a) and (b) are adapted from [12].

### C. Feasibility of $2e$ -ARPES measurements in $\text{FeSe}_{0.45}\text{Te}_{0.55}$

We note that our findings are directly applicable to the case of  $\text{FeSe}_{0.45}\text{Te}_{0.55}$  to distinguish between the recently proposed 2DTSC [29,30] and 3DTI [12,22–24] mechanisms for the emergence of topological surface superconductivity. As discussed in [41,49], a possible configuration for  $2e$ -ARPES experiments is the use of two time-of-flight (TOF) analyzers placed orthogonal to each other, with an XUV photon beam normally incident onto the sample under study. In this configuration,  $2e$ -ARPES can explicitly probe both the holelike and electronlike Fermi surfaces of  $\text{FeSe}_{0.45}\text{Te}_{0.55}$  using two TOF analyzers and XUV photon energies of 9 and 21 eV [as illustrated in Figs. 5(a) and 5(b)]. This calculation is based on the standard formulas relating the angle at which an electron is photoemitted to its in-plane momentum in the material, i.e.,  $k_{\parallel} = \frac{\sqrt{2m}}{\hbar} \sqrt{E_k} \sin \theta$  [48]. Figures 5(a) and 5(b) illustrate that both the holelike and electronlike Fermi surfaces in  $\text{FeSe}_{0.45}\text{Te}_{0.55}$  can be measured independently of each other by varying the incident photon energy.

## IV. CONCLUSIONS

We have demonstrated that  $2e$ -ARPES experiments can detect superconducting spin-triplet correlations that are induced in a 2DTSC, even in the absence of an associated long-range order parameter. This allows us to identify characteristic signatures in the  $2e$ -ARPES photoelectron counting rate  $P^{(2)}$  for equal spin configuration that distinguish between the recently proposed 2DTSC [29,30] and 3DTI [12,22–24] mechanisms for the emergence of topological surface superconductivity in  $\text{FeSe}_{0.45}\text{Te}_{0.55}$ . Finally, we showed that  $P_{SC}^{(2)}$  exhibits a characteristic feature—a maximum in intensity—at a topological phase transition that allows one to identify its occurrence. These results show that  $2e$ -ARPES spectroscopy represents an invaluable experimental probe in the study of topological superconductors.

## ACKNOWLEDGMENTS

This study was supported by the Center for Quantum Sensing and Quantum Materials, an Energy Frontier Research Center funded by the U.S. Department of Energy,

Office of Science, Basic Energy Sciences under Grant No. DE-SC0021238. F.M. acknowledges support from the EPiQS program of the Gordon and Betty Moore Foundation, Grant No. GBMF11069.

## APPENDIX A: PHOTOELECTRON COUNTING RATE FROM 2DTSC

To compute  $P^2$ , we start from Eq. (6), assuming that a photon beam is incident for times  $-\Delta t/2 \leq t \leq \Delta t/2$ . As discussed in the main text, the photon momentum  $\mathbf{q}$  is much smaller than typical fermionic momenta, and we therefore set it equal to zero, such that  $\gamma_\nu(\mathbf{q}) = \gamma_0$  is simply a momentum-independent constant. We then have

$$\begin{aligned} \langle \Psi_b | \hat{S}^{(2)}(\infty, -\infty) | \Psi_a \rangle &= \int_{-\Delta t/2}^{\Delta t/2} dt_2 \int_{t_2}^{\infty} dt_1 \sum_{\mathbf{k}_1, \sigma_1} \sum_{\mathbf{k}_2, \sigma_2} \sum_{\mathbf{k}_3, \sigma_3} \sum_{\mathbf{p}} \gamma_0 V(\mathbf{p}) \\ &\times \langle \Psi_b | d_{\mathbf{k}_2+\mathbf{p}, \sigma_2}^\dagger(t_1) d_{\mathbf{k}_3-\mathbf{p}, \sigma_3}^\dagger(t_1) d_{\mathbf{k}_3, \sigma_3}(t_1) c_{\mathbf{k}_2, \sigma_2}(t_1) d_{\mathbf{k}_1, \sigma_1}^\dagger(t_2) c_{\mathbf{k}_1, \sigma_1}(t_2) a_{\mathbf{q}=0, \lambda}(t_2) | \Psi_a \rangle. \end{aligned} \quad (\text{A1})$$

The last term in the integrand can then be simplified as

$$\begin{aligned} &\langle \Psi_b | d_{\mathbf{k}_2+\mathbf{p}, \sigma_2}^\dagger(t_1) d_{\mathbf{k}_3-\mathbf{p}, \sigma_3}^\dagger(t_1) d_{\mathbf{k}_3, \sigma_3}(t_1) c_{\mathbf{k}_2, \sigma_2}(t_1) d_{\mathbf{k}_1, \sigma_1}^\dagger(t_2) c_{\mathbf{k}_1, \sigma_1}(t_2) a_{\mathbf{q}=0, \lambda}(t_2) | \Psi_a \rangle \\ &= \langle 1_{\mathbf{k}_1, \sigma_1}^\dagger 1_{\mathbf{k}_2, \sigma_2}^\dagger | d_{\mathbf{k}_2+\mathbf{p}, \sigma_2}^\dagger(t_1) d_{\mathbf{k}_3-\mathbf{p}, \sigma_3}^\dagger(t_1) d_{\mathbf{k}_3, \sigma_3}(t_1) d_{\mathbf{k}_1, \sigma_1}^\dagger(t_2) | 0 \rangle \langle \Phi_b | c_{\mathbf{k}_2, \sigma_2}(t_1) c_{\mathbf{k}_1, \sigma_1}(t_2) | \Phi_a \rangle \langle 0 | a_{\mathbf{q}=0, \lambda}(t_2) | 1_{\mathbf{q}=0, \lambda} \rangle \\ &= e^{i(\epsilon_{\mathbf{k}_2+\mathbf{p}} + \epsilon_{\mathbf{k}_3-\mathbf{p}} - \epsilon_{\mathbf{k}_3})t_1} e^{i\epsilon_{\mathbf{k}_1}t_2} [\delta_{\mathbf{k}_1', \mathbf{k}_3-\mathbf{p}} \delta_{\sigma_1', \sigma_3} \delta_{\mathbf{k}_2', \mathbf{k}_2+\mathbf{p}} \delta_{\sigma_2', \sigma_2} - \delta_{\mathbf{k}_1', \mathbf{k}_2+\mathbf{p}} \delta_{\sigma_1', \sigma_2} \delta_{\mathbf{k}_2', \mathbf{k}_3-\mathbf{p}} \delta_{\sigma_2', \sigma_3}] \\ &\times \delta_{\mathbf{k}_3, \mathbf{k}_1} \delta_{\sigma_3, \sigma_1} e^{-i\omega_{\mathbf{q}2}} \langle \Phi_b | c_{\mathbf{k}_2, \sigma_2}(t_1) c_{\mathbf{k}_1, \sigma_1}(t_2) | \Phi_a \rangle \end{aligned} \quad (\text{A2})$$

where  $\epsilon_{\mathbf{k}}$  is the energy of a photoelectron with momentum  $\mathbf{k}$ . Using the spinor  $\Psi_{\mathbf{k}}^\dagger = (c_{\mathbf{k}, \uparrow}^\dagger, c_{\mathbf{k}, \downarrow}^\dagger, c_{-\mathbf{k}, \downarrow}, c_{-\mathbf{k}, \uparrow})$ , we rewrite Eq. (1) in matrix form as  $H = \sum_{\mathbf{k}} \Psi_{\mathbf{k}}^\dagger \hat{H}_{\mathbf{k}} \Psi_{\mathbf{k}}$  and diagonalize it using the Bogoliubov transformation

$$\Psi_{\mathbf{k}}^\dagger = (c_{\mathbf{k}, \uparrow}^\dagger, c_{\mathbf{k}, \downarrow}^\dagger, c_{-\mathbf{k}, \downarrow}, c_{-\mathbf{k}, \uparrow}) = (\gamma_{1, \mathbf{k}}^\dagger, \gamma_{2, \mathbf{k}}^\dagger, \gamma_{3, \mathbf{k}}^\dagger, \gamma_{4, \mathbf{k}}^\dagger) \hat{U}_{\mathbf{k}}^\dagger = \Gamma_{\mathbf{k}}^\dagger \hat{U}_{\mathbf{k}}^\dagger, \quad \Psi_{\mathbf{k}} = \begin{pmatrix} c_{\mathbf{k}, \uparrow} \\ c_{\mathbf{k}, \downarrow} \\ c_{-\mathbf{k}, \downarrow} \\ c_{-\mathbf{k}, \uparrow} \end{pmatrix} = \hat{U}_{\mathbf{k}} \begin{pmatrix} \gamma_{1, \mathbf{k}} \\ \gamma_{2, \mathbf{k}} \\ \gamma_{3, \mathbf{k}} \\ \gamma_{4, \mathbf{k}} \end{pmatrix} = \hat{U}_{\mathbf{k}} \Gamma_{\mathbf{k}} \quad (\text{A3})$$

where  $\hat{U}_{\mathbf{k}}$  is a unitary matrix consisting of the eigenvectors of  $\hat{H}_{\mathbf{k}}$ . This yields

$$H = \sum_{\mathbf{k}} \Psi_{\mathbf{k}}^\dagger \hat{H}_{\mathbf{k}} \Psi_{\mathbf{k}} = \sum_{\mathbf{k}} \Gamma_{\mathbf{k}}^\dagger \hat{U}_{\mathbf{k}}^\dagger \hat{H}_{\mathbf{k}} \hat{U}_{\mathbf{k}} \Gamma_{\mathbf{k}} = \sum_{\mathbf{k}} \Gamma_{\mathbf{k}}^\dagger \hat{E}_{\mathbf{k}} \Gamma_{\mathbf{k}} \quad (\text{A4})$$

where

$$\hat{E}_{\mathbf{k}} = \begin{pmatrix} E_{1, \mathbf{k}} & 0 & 0 & 0 \\ 0 & E_{2, \mathbf{k}} & 0 & 0 \\ 0 & 0 & E_{3, \mathbf{k}} & 0 \\ 0 & 0 & 0 & E_{4, \mathbf{k}} \end{pmatrix} \quad (\text{A5})$$

and  $E_{i, \mathbf{k}} (i = 1, \dots, 4)$  are the eigenenergies of  $\hat{H}_{\mathbf{k}}$ . In the main text, we took the photoelectron momenta to be opposite, such that  $\mathbf{k}'_2 = -\mathbf{k}'_1$ . Using the Bogoliubov transformation of Eq. (A3) to simplify the last term in Eq. (A2), we then obtain from Eqs. (6) and (A1) after taking the limit  $\Delta t \rightarrow \infty$  that  $P^{(2)} = V^2 P_{\text{SC}}^{(2)} + V P_{\text{2CP}}^{(2)}$  where

$$\begin{aligned} P_{\text{SC}}^{(2)}(\mathbf{k}'_1, \sigma'_1, \sigma'_2) &= 2\pi \gamma_0^2 \delta(2\epsilon_{\mathbf{k}'_1} - \omega_0) \left| \sum_{\mathbf{k}} \sum_{i=1}^4 [U_{\mathbf{k}}]_{ni} [U_{\mathbf{k}}]_{mi}^* \left[ \frac{V(\mathbf{k} - \mathbf{k}'_1) n_F(E_{i, \mathbf{k}})}{2\epsilon_{\mathbf{k}'_1} - \epsilon_{\mathbf{k}} + E_{i, \mathbf{k}} + i\delta} - \frac{V(\mathbf{k} - \mathbf{k}'_1) [1 - n_F(E_{i, \mathbf{k}})]}{2\epsilon_{\mathbf{k}'_1} - \epsilon_{\mathbf{k}} - E_{i, \mathbf{k}} + i\delta} \right] \right|^2, \\ P_{\text{2CP}}^{(2)}(\mathbf{k}'_1, \sigma'_1, \sigma'_2) &= 2\pi \gamma_0^2 \sum_{\mathbf{k}} \sum_{i, j=1}^4 |[U_{\mathbf{k}}]_{ni}|^2 |[U_{\mathbf{k}}]_{mj}|^2 \delta(2\epsilon_{\mathbf{k}'_1} - \omega + E_{i, \mathbf{k}} - E_{j, \mathbf{k}}) \\ &\times \left| \frac{V(\mathbf{k} - \mathbf{k}'_1)}{2\epsilon_{\mathbf{k}'_1} - \epsilon_{\mathbf{k}} + E_{i, \mathbf{k}} + i\delta} + \frac{V(\mathbf{k} - \mathbf{k}'_1)}{2\epsilon_{\mathbf{k}'_1} - \epsilon_{\mathbf{k}} - E_{j, \mathbf{k}} + i\delta} \right|^2 [1 - n_F(E_{i, \mathbf{k}})] n_F(E_{j, \mathbf{k}}) \end{aligned} \quad (\text{A6})$$

where  $n = 1, 2$  for  $\sigma'_1 = \uparrow, \downarrow$  and  $m = 4, 3$  for  $\sigma'_2 = \uparrow, \downarrow$ .

### APPENDIX B: PHOTOELECTRON COUNTING RATE FROM 3DTI

To compute the photoelectron counting rate for the 3DTI system, we need to consider a slab geometry, since the Dirac cone only emerges on the surface layer of the system. To this end, we perform a partial Fourier transform of the Hamiltonian in Eqs. (2) and (4) from real space  $(x, y, z)$  to  $(k_x, k_y, z)$ . Since ARPES is a surface sensitive probe, we assume that the interaction between the incident photon, conduction electrons, and photoelectrons occurs only on the surface layer of the system, denoted by  $z = 1$ . The scattering Hamiltonian is then given by

$$H_{\text{scat}} = \sum_{\mathbf{k}, \mathbf{q}, \sigma, \nu} \gamma_\nu(\mathbf{q}) d_{\mathbf{k}+\mathbf{q}, \sigma}^\dagger c_{\mathbf{k}, z=1, m_1, \sigma} (a_{\mathbf{q}, \nu} + a_{-\mathbf{q}, \nu}^\dagger) + \sum_{\mathbf{k}, \mathbf{p}, \mathbf{q}, \alpha, \beta} V(\mathbf{q}) d_{\mathbf{k}+\mathbf{q}, \alpha}^\dagger d_{\mathbf{p}-\mathbf{q}, \beta}^\dagger d_{\mathbf{p}, \beta} c_{\mathbf{k}, z=1, m_2, \alpha} + \text{H.c.} \quad (\text{B1})$$

with  $m_{1,2}$  denoting the orbital index. The derivation of  $P^{(2)}$  is then similar to that in the 2DTSC system, with the exception that we now have a layer index  $z$  and orbital indices  $m_{1,2}$ . As a result, the scattering amplitude  $\langle \Phi_b | c_{\mathbf{k}_2, \sigma_2}(t_1) c_{\mathbf{k}_1, \sigma_1}(t_2) | \Phi_a \rangle$  in Eq. (A2) needs to be generalized to

$$\langle \Phi_b | c_{\mathbf{k}_2, z=1, m_2, \sigma_2}(t_1) c_{\mathbf{k}_1, z=1, m_1, \sigma_1}(t_2) | \Phi_a \rangle. \quad (\text{B2})$$

We next rewrite the 3DTI Hamiltonian in matrix form and diagonalize it via

$$H_{3\text{D}} = \sum_{\mathbf{k}} \Psi_{\mathbf{k}}^\dagger \hat{H}_{\mathbf{k}} \Psi_{\mathbf{k}} = \sum_{\mathbf{k}} \Gamma_{\mathbf{k}}^\dagger \hat{U}_{\mathbf{k}}^\dagger \hat{H}_{\mathbf{k}} \hat{U}_{\mathbf{k}} \Gamma_{\mathbf{k}} = \sum_{\mathbf{k}} \Gamma_{\mathbf{k}}^\dagger \hat{E}_{\mathbf{k}} \Gamma_{\mathbf{k}} \quad (\text{B3})$$

where  $\mathbf{k} = (k_x, k_y)$ , and we defined the spinor

$$\Psi_{\mathbf{k}}^\dagger = (\psi_{\mathbf{k}, z=1}^\dagger \quad \cdots \quad \psi_{\mathbf{k}, z=N_z}^\dagger), \quad (\text{B4})$$

$$\psi_{\mathbf{k}, z}^\dagger = (c_{\mathbf{k}, z, 1, \uparrow}^\dagger \quad c_{\mathbf{k}, z, 2, \uparrow}^\dagger \quad c_{\mathbf{k}, z, 1, \downarrow}^\dagger \quad c_{\mathbf{k}, z, 2, \downarrow}^\dagger \quad c_{-\mathbf{k}, z, 1, \uparrow} \quad c_{-\mathbf{k}, z, 2, \uparrow} \quad c_{-\mathbf{k}, z, 1, \downarrow} \quad c_{-\mathbf{k}, z, 2, \downarrow}). \quad (\text{B5})$$

Moreover, the Bogoliubov transformation is given by

$$\Psi_{\mathbf{k}} = \begin{pmatrix} \psi_{\mathbf{k}, z=1} \\ \vdots \\ \psi_{\mathbf{k}, z=N_z} \end{pmatrix} = \hat{U}_{\mathbf{k}} \begin{pmatrix} \gamma_{1, \mathbf{k}} \\ \vdots \\ \gamma_{8N_z, \mathbf{k}} \end{pmatrix} = \hat{U}_{\mathbf{k}} \Gamma_{\mathbf{k}} \quad (\text{B6})$$

where  $\hat{U}_{\mathbf{k}}$  is the unitary matrix consisting of the eigenvectors of  $\hat{H}_{\mathbf{k}}$ . Using the Bogoliubov transformation of Eq. (B6) to simplify the term in Eq. (B2), we then obtain from Eqs. (6) and (A1) after taking the limit  $\Delta t \rightarrow \infty$  and for  $\mathbf{k}'_2 = -\mathbf{k}'_1$  that

$$P^{(2)}(\mathbf{k}'_1, m_1, \sigma'_1, m_2, \sigma'_2) = V^2 P_{\text{SC}}^{(2)}(\mathbf{k}'_1, m_1, \sigma'_1, m_2, \sigma'_2) + V P_{2\text{CP}}^{(2)}(\mathbf{k}'_1, m_1, \sigma'_1, m_2, \sigma'_2) \quad (\text{B7})$$

where

$$P_{\text{SC}}^{(2)} = 2\pi \gamma_0^2 \delta(2\epsilon_{\mathbf{k}'_1} - \omega) \left| \sum_{\mathbf{k}} \sum_{i=1}^{8N_z} [U_{\mathbf{k}}]_{4+n(m_2, \sigma'_2), i}^* [U_{\mathbf{k}}]_{n(m_1, \sigma'_1), i} \left[ \frac{V(\mathbf{k} - \mathbf{k}'_1) n_F(E_{i, \mathbf{k}})}{2\epsilon_{\mathbf{k}'_1} - \epsilon_{\mathbf{k}} + E_{i, \mathbf{k}} + i\delta} - \frac{V(\mathbf{k} - \mathbf{k}'_1) [1 - n_F(E_{i, \mathbf{k}})]}{2\epsilon_{\mathbf{k}'_1} - \epsilon_{\mathbf{k}} - E_{i, \mathbf{k}} + i\delta} \right] \right|^2,$$

$$P_{2\text{CP}}^{(2)} = 2\pi \gamma_0^2 \sum_{\mathbf{k}} \sum_{i, j=1}^{8N_z} \left| [U_{\mathbf{k}}]_{4+n(m_2, \sigma'_2), i} \right|^2 \left| [U_{\mathbf{k}}]_{n(m_1, \sigma'_1), j} \right|^2 \delta(2\epsilon_{\mathbf{k}'_1} - \omega + E_{i, \mathbf{k}} - E_{j, \mathbf{k}})$$

$$\times \left| \frac{V(\mathbf{k} - \mathbf{k}'_1)}{2\epsilon_{\mathbf{k}'_1} - \epsilon_{\mathbf{k}} + E_{i, \mathbf{k}} + i\delta} + \frac{V(\mathbf{k} - \mathbf{k}'_1)}{2\epsilon_{\mathbf{k}'_1} - \epsilon_{\mathbf{k}} - E_{j, \mathbf{k}} + i\delta} \right|^2 [1 - n_F(E_{i, \mathbf{k}})] n_F(E_{j, \mathbf{k}}), \quad (\text{B8})$$

and

$$n_{(m, \sigma)} = \begin{cases} 1 & , (m, \sigma) = (1, \uparrow) \\ 2 & , (m, \sigma) = (2, \uparrow) \\ 3 & , (m, \sigma) = (1, \downarrow) \\ 4 & , (m, \sigma) = (2, \downarrow) \end{cases}$$

### APPENDIX C: SUPERCONDUCTING SPIN-TRIPLET CORRELATIONS NEAR A TOPOLOGICAL PHASE TRANSITION

We showed in Fig. 3 that the peak in  $P_{\text{SC}}^{(2)}$  at the topological phase transition reflects the peak in the superconducting spin-triplet correlations. To derive an analytical form for these correlations, we use the structure of the Hamiltonian matrix near the gap

closing points, which are given by  $\mathbf{k}_{\text{gc}} = (0, \pm\pi)$ ,  $(\pm\pi, 0)$  for the transition between the trivial  $C = 0$  and  $-1$  phases (case 1) and by  $\mathbf{k}_{\text{gc}} = (\pm\pi, \pm\pi)$  for the transition between the trivial  $C = 0$  and 2 phases (case 2). Specifically, considering these phase transitions with  $\mu = 0$  and  $4t$  for case 1 and 2, respectively, we have  $\xi_{\mathbf{k}_{\text{gc}}=0}$ . Thus, to linear order in the deviation from the gap closing momentum  $\mathbf{k}_{\text{gc}}$ , the Hamiltonian matrix is given by

$$\hat{H} = \begin{pmatrix} -J & -A_{\mathbf{k}} & \Delta & 0 \\ -A_{\mathbf{k}}^* & J & 0 & -\Delta \\ \Delta & 0 & -J & -A_{\mathbf{k}} \\ 0 & -\Delta & -A_{\mathbf{k}}^* & J \end{pmatrix} \quad (\text{C1})$$

where  $A_{\mathbf{k}} = 2\alpha(\sin k_x + i \sin k_y)$ .

Diagonalizing the Hamiltonian matrix yields the following eigenenergies ( $i = 1, \dots, 4$ ):

$$E_i = \pm\sqrt{(\Delta \pm J)^2 + |A_{\mathbf{k}}|^2}. \quad (\text{C2})$$

Next, we compute the triplet correlations:

$$C_{T,\uparrow} = \langle c_{-\mathbf{k},\uparrow} c_{\mathbf{k},\uparrow} \rangle = \sum_i [\hat{U}_{\mathbf{k}}]_{1i} [\hat{U}_{\mathbf{k}}]_{4i}^* n_F(E_{i,\mathbf{k}}). \quad (\text{C3})$$

At  $T = 0$  only states with negative energies  $E_{1,2} = -\sqrt{(\Delta \pm J)^2 + |A_{\mathbf{k}}|^2}$  contribute to  $C_{T,\uparrow}$ . These energy states possess the normalized eigenvectors

$$\begin{aligned} \Phi_1 &= \frac{1}{\sqrt{2\left[1 + \frac{[\sqrt{(\Delta+J)^2 + |A_{\mathbf{k}}|^2} + \Delta + J]^2}{|A_{\mathbf{k}}|^2}\right]}} \left( -\frac{\sqrt{(\Delta+J)^2 + |A_{\mathbf{k}}|^2} + \Delta + J}{A_{\mathbf{k}}^*}, -1, \frac{\sqrt{(\Delta+J)^2 + |A_{\mathbf{k}}|^2} + \Delta + J}{A_{\mathbf{k}}^*}, 1 \right), \\ \Phi_2 &= \frac{1}{\sqrt{2\left[1 + \frac{[\sqrt{(\Delta-J)^2 + |A_{\mathbf{k}}|^2} - (\Delta - J)]^2}{|A_{\mathbf{k}}|^2}\right]}} \left( \frac{\sqrt{(\Delta-J)^2 + |A_{\mathbf{k}}|^2} - (\Delta - J)}{A_{\mathbf{k}}^*}, 1, \frac{\sqrt{(\Delta-J)^2 + |A_{\mathbf{k}}|^2} - (\Delta - J)}{A_{\mathbf{k}}^*}, 1 \right). \end{aligned} \quad (\text{C4})$$

We thus obtain at  $T = 0$

$$\begin{aligned} C_{\mathbf{k},\uparrow}^T &= [\hat{U}_{\mathbf{k}}]_{11} [\hat{U}_{\mathbf{k}}]_{41}^* + [\hat{U}_{\mathbf{k}}]_{12} [\hat{U}_{\mathbf{k}}]_{42}^* = -\frac{\sqrt{(\Delta+J)^2 + |A_{\mathbf{k}}|^2} + \Delta + J}{2\{|A_{\mathbf{k}}|^2 + [\sqrt{(\Delta+J)^2 + |A_{\mathbf{k}}|^2} + \Delta + J]^2\}} A_{\mathbf{k}} \\ &\quad + \frac{\sqrt{(\Delta-J)^2 + |A_{\mathbf{k}}|^2} - (\Delta - J)}{2\{|A_{\mathbf{k}}|^2 + [\sqrt{(\Delta-J)^2 + |A_{\mathbf{k}}|^2} - (\Delta - J)]^2\}} A_{\mathbf{k}} \end{aligned} \quad (\text{C5})$$

with the second term being the dominant one near the gap closing. To understand the origin of the peak in the superconducting spin-triplet correlations in more detail, we expand the above expression for  $|A_{\mathbf{k}}| \ll \Delta - J$ , which yields to leading order in  $|A_{\mathbf{k}}|$

$$C_{\mathbf{k},\uparrow}^T \approx \frac{|A_{\mathbf{k}}|}{4(\Delta - J)}. \quad (\text{C6})$$

Comparing this with the known result for the spin-singlet correlations in a conventional  $s$ -wave superconductor  $C_{\mathbf{k}}^S = \Delta/E_{\mathbf{k}}$ , where  $E_{\mathbf{k}}$  is the energy dispersion in the superconducting state, we infer that  $A_{\mathbf{k}}$  in Eq. (C6) corresponds to the induced spin-triplet gap, while  $(\Delta - J)$  is the excitation energy as expected from Eq. (C2). We can thus conclude that the reason for the increase of the spin-triplet correlations as one approaches the gap closing, and thus for the peak in  $P_{\text{SC}}^{(2)}$  at the phase transition, is the decrease in the excitation energy  $(\Delta - J)$ .

In Fig. 6, we present a comparison between the numerically obtained triplet correlations  $|C_{\mathbf{k},\uparrow}^T|$ , and the analytical form of the triplet correlations obtained from Eq. (C5), for two different momenta near the gap closing momentum  $\mathbf{k}_{\text{gc}} = (0, \pm\pi)$ . The good agreement between these two results confirmed the validity of the analytical form shown in Eq. (C5).

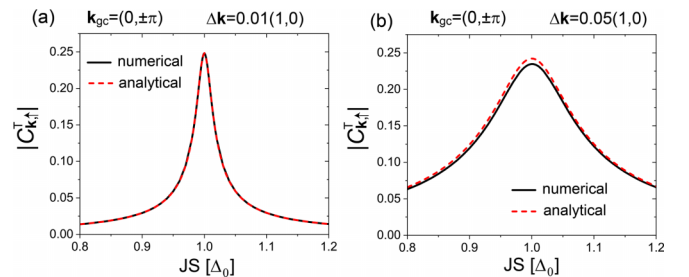


FIG. 6. (a, b) Comparison between the numerical and analytical results for  $|C_{\mathbf{k},\uparrow}^T|$  for two different momenta near the gap closing momentum  $\mathbf{k}_{\text{gc}} = (0, \pm\pi)$ .

- [1] C. Nayak, S. H. Simon, A. Stern, M. Freedman, and S. Das Sarma, *Rev. Mod. Phys.* **80**, 1083 (2008).
- [2] V. Mourik, K. Zuo, S. M. Frolov, S. R. Plissard, E. P. A. M. Bakkers, and L. P. Kouwenhoven, *Science* **336**, 1003 (2012).
- [3] S. Nadj-Perge, I. K. Drozdov, J. Li, H. Chen, S. Jeon, J. Seo, A. H. MacDonald, B. A. Bernevig, and A. Yazdani, *Science* **346**, 602 (2014).
- [4] A. Das, Y. Ronen, Y. Most, Y. Oreg, M. Heiblum, and H. Shtrikman, *Nat. Phys.* **8**, 887 (2012).
- [5] M. Ruby, F. Pientka, Y. Peng, F. von Oppen, B. W. Heinrich, and K. J. Franke, *Phys. Rev. Lett.* **115**, 197204 (2015).
- [6] R. Pawlak, M. Kisiel, J. Klinovaja, T. Meier, S. Kawai, T. Glatzel, D. Loss, and E. Meyer, *npj Quantum Inf.* **2**, 16035 (2016).
- [7] H. Kim, A. Palacio-Morales, T. Posske, L. Rózsa, K. Palotás, L. Szunyogh, M. Thorwart, and R. Wiesendanger, *Sci. Adv.* **4**, eaar5251 (2018).
- [8] S. Manna, P. Wei, Y. Xie, K. T. Law, P. A. Lee, and J. S. Moodera, *Proc. Natl. Acad. Sci. USA* **117**, 8775 (2020).
- [9] G. C. Ménard, S. Guissart, C. Brun, R. T. Leriche, M. Trif, F. Debontridder, D. Demaille, D. Roditchev, P. Simon, and T. Cren, *Nat. Commun.* **8**, 2040 (2017).
- [10] A. Palacio-Morales, E. Mascot, S. Cocklin, H. Kim, S. Rachel, D. K. Morr, and R. Wiesendanger, *Sci. Adv.* **5**, eaav6600 (2019).
- [11] G. C. Ménard, A. Mesaros, C. Brun, F. Debontridder, D. Roditchev, P. Simon, and T. Cren, *Nat. Commun.* **10**, 2587 (2019).
- [12] P. Zhang, K. Yaji, T. Hashimoto, Y. Ota, T. Kondo, K. Okazaki, Z. Wang, J. Wen, G. D. Gu, H. Ding, and S. Shin, *Science* **360**, 182 (2018).
- [13] J. D. Rameau, N. Zaki, G. D. Gu, P. D. Johnson, and M. Weinert, *Phys. Rev. B* **99**, 205117 (2019).
- [14] N. Zaki, G. Gu, A. Tselik, C. Wu, and P. D. Johnson, *Proc. Natl. Acad. Sci. USA* **118**, e2007241118 (2021).
- [15] Y. Li, N. Zaki, V. O. Garlea, A. T. Savici, D. Fobes, Z. Xu, F. Camino, C. Petrovic, G. Gu, P. D. Johnson, J. M. Tranquada, and I. A. Zaliznyak, *Nat. Mat.* **20**, 1221 (2021).
- [16] D. Wang, L. Kong, P. Fan, H. Chen, S. Zhu, W. Liu, L. Cao, Y. Sun, S. Du, J. Schneeloch, R. Zhong, G. Gu, L. Fu, H. Ding, and H.-J. Gao, *Science* **362**, 333 (2018).
- [17] T. Machida, Y. Sun, S. Pyon, S. Takeda, Y. Kohsaka, T. Hanaguri, T. Sasagawa, and T. Tamegai, *Nat. Mater.* **18**, 811 (2019).
- [18] L. Kong, S. Zhu, M. Papaj, H. Chen, L. Cao, H. Isobe, Y. Xing, W. Liu, D. Wang, P. Fan, Y. Sun, S. Du, J. Schneeloch, R. Zhong, G. Gu, L. Fu, H.-J. Gao, and H. Ding, *Nat. Phys.* **15**, 1181 (2019).
- [19] S. Zhu, L. Kong, L. Cao, H. Chen, M. Papaj, S. Du, Y. Xing, W. Liu, D. Wang, C. Shen, F. Yang, J. Schneeloch, R. Zhong, G. Gu, L. Fu, Y.-Y. Zhang, H. Ding, and H.-J. Gao, *Science* **367**, 189 (2020).
- [20] C. Chen, K. Jiang, Y. Zhang, C. Liu, Y. Liu, Z. Wang, and J. Wang, *Nat. Phys.* **16**, 536 (2020).
- [21] Z. Wang, J. O. Rodriguez, L. Jiao, S. Howard, M. Graham, G. D. Gu, T. L. Hughes, D. K. Morr, and V. Madhavan, *Science* **367**, 104 (2020).
- [22] Z. Wang, P. Zhang, G. Xu, L. K. Zeng, H. Miao, X. Xu, T. Qian, H. Weng, P. Richard, A. V. Fedorov, H. Ding, X. Dai, and Z. Fang, *Phys. Rev. B* **92**, 115119 (2015).
- [23] X. Wu, S. Qin, Y. Liang, H. Fan, and J. Hu, *Phys. Rev. B* **93**, 115129 (2016).
- [24] G. Xu, B. Lian, P. Tang, X.-L. Qi, and S.-C. Zhang, *Phys. Rev. Lett.* **117**, 047001 (2016).
- [25] L. Fu and C. L. Kane, *Phys. Rev. Lett.* **100**, 096407 (2008).
- [26] N. J. McLaughlin, H. Wang, M. Huang, E. Lee-Wong, L. Hu, H. Lu, G. Q. Yan, G. Gu, C. Wu, Y.-Z. You, and C. R. Du, *Nano Lett.* **21**, 7277 (2021).
- [27] X. Wu, S. B. Chung, C. Liu, and E.-A. Kim, *Phys. Rev. Res.* **3**, 013066 (2021).
- [28] C. Xu, K. H. Wong, E. Mascot, and D. K. Morr, *Phys. Rev. B* **107**, 214514 (2023).
- [29] E. Mascot, S. Cocklin, M. Graham, M. Mashkooori, S. Rachel, and D. K. Morr, *Commun. Phys.* **5**, 188 (2022).
- [30] K. H. Wong, E. Mascot, V. Madhavan, D. J. Van Harlingen, and D. K. Morr, *Phys. Rev. B* **105**, L220504 (2022).
- [31] J. Berakdar, *Phys. Rev. B* **58**, 9808 (1998).
- [32] F. Mahmood, T. Devereaux, P. Abbamonte, and D. K. Morr, *Phys. Rev. B* **105**, 064515 (2022).
- [33] J. Röntynen and T. Ojanen, *Phys. Rev. Lett.* **114**, 236803 (2015).
- [34] J. Li, T. Neupert, Z. Wang, A. H. MacDonald, A. Yazdani, and B. A. Bernevig, *Nat. Commun.* **7**, 12297 (2016).
- [35] S. Rachel, E. Mascot, S. Cocklin, M. Vojta, and D. K. Morr, *Phys. Rev. B* **96**, 205131 (2017).
- [36] H. Miao, P. Richard, Y. Tanaka, K. Nakayama, T. Qian, K. Umezawa, T. Sato, Y.-M. Xu, Y. B. Shi, N. Xu, X.-P. Wang, P. Zhang, H.-B. Yang, Z.-J. Xu, J. S. Wen, G.-D. Gu, X. Dai, J.-P. Hu, T. Takahashi, and H. Ding, *Phys. Rev. B* **85**, 094506 (2012).
- [37] M. Sato, Y. Takahashi, and S. Fujimoto, *Phys. Rev. Lett.* **103**, 020401 (2009).
- [38] J. D. Sau, R. M. Lutchyn, S. Tewari, and S. Das Sarma, *Phys. Rev. Lett.* **104**, 040502 (2010).
- [39] G. Schubert, H. Fehske, L. Fritz, and M. Vojta, *Phys. Rev. B* **85**, 201105(R) (2012).
- [40] H. W. Haak, G. A. Sawatzky, and T. D. Thomas, *Phys. Rev. Lett.* **41**, 1825 (1978).
- [41] C.-T. Chiang, A. Trützschler, M. Huth, R. Kamrula, F. O. Schumann, and W. Widdra, *Prog. Surf. Sci.* **95**, 100572 (2020).
- [42] N. Fominykh, J. Berakdar, J. Henk, and P. Bruno, *Phys. Rev. Lett.* **89**, 086402 (2002).
- [43] F. O. Schumann, C. Winkler, and J. Kirschner, *Phys. Rev. Lett.* **98**, 257604 (2007).
- [44] F. O. Schumann, R. S. Dhaka, G. A. van Riessen, Z. Wei, and J. Kirschner, *Phys. Rev. B* **84**, 125106 (2011).
- [45] F. O. Schumann, L. Behnke, C. H. Li, J. Kirschner, Y. Pavlyukh, and J. Berakdar, *Phys. Rev. B* **86**, 035131 (2012).
- [46] R. Herrmann, S. Samarin, H. Schwabe, and J. Kirschner, *Phys. Rev. Lett.* **81**, 2148 (1998).
- [47] E. Mascot, J. Bedow, M. Graham, S. Rachel, and D. K. Morr, *npj Quantum Mater.* **6**, 6 (2021).
- [48] J. A. Sobota, Y. He, and Z.-X. Shen, *Rev. Mod. Phys.* **93**, 025006 (2021).
- [49] J. Zwettler, H. Amir, F. H. Marashi, N. Bielinski, S. Patel, P. Mahaadev, Y. Huang, D. Chaudhuri, X. Guo, T. C. Chiang, D. K. Morr, P. Abbamonte, and F. Mahmood, *J. Electron Spectrosc. Relat. Phenom.* **270**, 147417 (2024).